

# DEVELOPMENT AND TESTING OF AN INTELLIGENT TOBACCO LEAF HARVESTING ROBOT BASED ON MACHINE VISION

## 基于机器视觉的智能烟叶采摘机器人开发与测试

YuPei LIN<sup>1,2</sup>, GuoYong YAN<sup>3</sup>, Tao WANG<sup>3</sup>, Tao BAI<sup>3</sup>, Si TANG<sup>3</sup>, JunJie CHEN<sup>\*1,2</sup>, BaoLin ZHANG <sup>\*3</sup>

<sup>1)</sup> Southwest University, College of Artificial Intelligence, Chongqing 400715, China

<sup>2)</sup> National & Local Joint Engineering Research Center of Intelligent Transmission and Control Technology, Chongqing 400715, China

<sup>3)</sup> Qujing Tobacco Company of Yunnan Province, Yunnan 655000, China

Tel: +86 13887482855; E-mail: 1031730720@qq.com; [13887482855@139.com](mailto:13887482855@139.com)

DOI: <https://doi.org/10.35633/inmateh-75-51>

**Keywords:** Tobacco Leaf Harvesting, Machine Vision, Robotic arm, Biomimetic flexible gripper, Kinematic Model

### ABSTRACT

The efficiency and quality of tobacco leaf harvesting are crucial for the economic performance of the tobacco industry. To enhance harvesting efficiency, a non-destructive tobacco leaf harvesting robot based on machine vision and robotics technology was developed. Experimental evaluations of key components demonstrated that the biomimetic flexible gripper based on the fin ray effect has good stiffness when the clamping force is 2.5 N, ensuring stable subsequent harvesting and collection of tobacco leaves. The introduction of a 6+1-axis robotic arm significantly expands the working range compared to the original 6-axis design, effectively covering the height of the tobacco stalk. The robotic arm's speed notably affects harvesting time ( $P < 0.001$ ), with 1.2 m/s identified as optimal for balancing recognition efficiency and success rates. Additionally, exposure time plays a critical role in success rates ( $P < 0.001$ ), achieving peaks of 90.00% in the morning and 83.33% in the afternoon at 40000  $\mu$ s. These advancements enhance tobacco harvesting technology and provide valuable insights for intelligent crop harvesting.

### 摘要

烟叶采摘的效率和质量对烟草行业的经济效益至关重要。为了提高采摘效率，基于机器视觉和机器人技术开发了一种无损烟叶采摘机器人。关键部件的实验评估表明，基于鳍条效应的仿生柔性夹爪在夹紧力为 2.5 N 时具有良好的刚度确保了后续烟叶采摘和回收的稳定性。引入的 6+1 轴机械臂相比原有的 6 轴设计，显著扩展了工作范围，有效覆盖了烟草柱的高度。机械臂的速度显著影响采摘时间 ( $P < 0.001$ )，1.2 m/s 的速度被确定为平衡识别效率和成功率的最佳值。此外，曝光时间对成功率也有关键作用 ( $P < 0.001$ )，上午和下午在 40000  $\mu$ s 时成功率分别达到 90.00% 和 83.33%。这些进展提升了烟叶采摘技术，并为农作物智能采摘提供了借鉴。

### INTRODUCTION

Tobacco leaves represent a significant economic crop, with a vast global market for planting and consumption (Liu S. X. et al, 2015). Harvesting tobacco leaves is a critical process in the tobacco production chain, where efficiency and quality directly influence the economic benefits of the tobacco industry (Bu L. X. et al, 2020). Currently, tobacco leaf harvesting is predominantly manual, characterized by high labor intensity, long hours, and substantial costs. Moreover, variations in subjective awareness and technical skills among workers can easily lead to damage and contamination of the leaves, adversely affecting both quality and yield (Xu Y. C. et al, 2016). The introduction of automated harvesting machinery has greatly improved efficiency. Research in this field led Li Yang et al, (2022) to develop a semi-automated tobacco harvesting machine, in which optimal parameters for the harvesting mechanism were determined through experimental trials, resulting in improved efficiency. However, the damage rate still exceeds 20%. Similarly, Ma Sijie et al, (2024), focused on designing and optimizing the key structures of automated tobacco harvesting machinery, employing experimental design methods to establish optimal harvesting parameters and successfully reducing the damage rate to below 10%, though this figure remains relatively high.

---

YuPei LIN, Ph.D. Eng.; GuoYong YAN, M.S. Eng.; Tao WANG, SA. Eng.; Tao BAI, M.S. Eng.; Si TANG, M.S. Eng.; JunJie CHEN, M.S. Eng.; BaoLin ZHANG, M.S. Eng.

Overall, existing bulk automated harvesting solutions often result in significant damage to tobacco leaves, limiting their practical application in production.

The integration of machine vision and robotic technology presents a promising solution for tobacco leaf harvesting (Jin Y. *et al*, 2020). Machine vision enables rapid identification and localization of leaf maturity, while robotic technology allows for precise execution of harvesting actions. This combination not only enhances the success rate of harvesting but also significantly reduces damage to the leaves, achieving an intelligent and precise harvesting process. While these technologies have been widely applied in harvesting other agricultural products (Shu Y. F. *et al*, 2024), their implementation in tobacco leaf harvesting remains rare (Zhi H.E. *et al*, 2023). The primary challenges in applying machine vision and robotics to tobacco harvesting include: 1) ensuring harvesting stability and effectiveness, which necessitates designing actuators with good enveloping characteristics and appropriate stiffness for damage-free harvesting; 2) achieving seamless integration of agronomy and machinery, requiring an organic combination of maturity identification and harvesting procedures to enhance efficiency; 3) maintaining high visual recognition success rates in complex environments, which involves breakthroughs in recognition technology, improvements in recognition efficiency, and methods for actuator matching.

To address these challenges, this study develops an intelligent, damage-free tobacco harvesting robot based on machine vision. The focus is on innovatively designing the end-effector structure for tobacco leaves, optimizing the harvesting path of the robot in conjunction with agronomy, and fine-tuning key parameters of the vision system through field tests to achieve a comprehensive solution for an efficient and stable tobacco harvesting system. This research not only advances tobacco harvesting technology, enhancing both efficiency and quality, but also provides valuable insights for the intelligent harvesting of other crops, holding significant practical application value.

## MATERIALS AND METHODS

### Machine structure and workflow

#### Machine structure

The developed intelligent, non-destructive tobacco harvesting robot, shown in Fig. 1, features a tracked mobility system, a 6+1-axis robotic arm, an end-effector, a depth camera, and a control system. The tracked mobility system ensures excellent terrain adaptability for flexible movement in complex agricultural environments, enhancing operational efficiency. The 6+1-axis robotic arm adds a vertical degree of freedom, allowing seamless integration with tobacco harvesting operations to improve efficiency. The end-effector employs a novel soft-hard gripping structure designed to maximize precision and efficiency while minimizing leaf damage. The control system integrates path planning, obstacle avoidance, and multi-task coordination, dynamically adjusting the arm's trajectory based on real-time visual feedback to ensure safety and stability. Its compact, modular design facilitates maintenance and upgrades, automating harvesting operations and enhancing intelligence through integrated vision and motion control, demonstrating significant application potential.

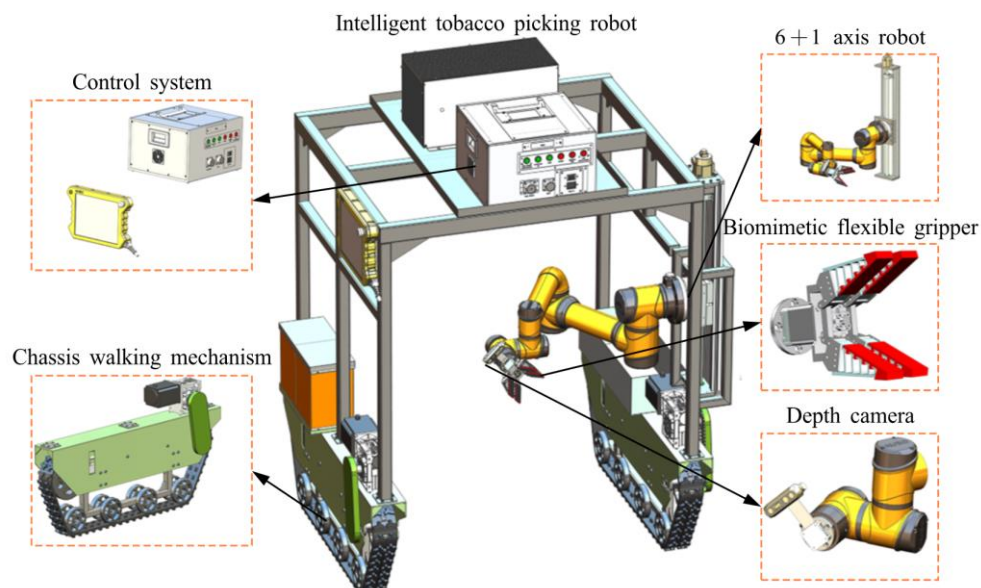


Fig. 1 – Machine Structure of the Tobacco Harvesting Robot

**Workflow**

The control system connects the end-effector, sliding device, robotic arm, and visual sensors via a central controller to facilitate automated and intelligent tobacco harvesting (Fig. 2). The process begins with program initiation, positioning the depth camera at the recognition point and issuing a recognition command. If obstructions are detected, the camera requests trajectory planning. The vision system identifies the petiole of the tobacco leaf, calculates the coordinates and angular orientation of the harvesting point, and transmits this data to the controller. The robotic arm then moves the end-effector to the harvesting point to complete the process. The system enters standby mode, ready to resume recognition and harvesting upon receiving new commands, concluding operations only when a stop command is issued.

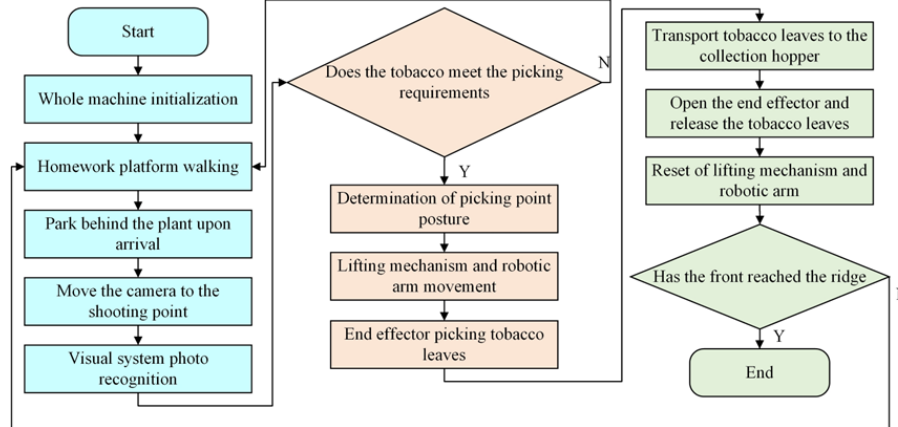


Fig. 2 – Workflow Diagram of the Tobacco Harvesting Robot

**Design and Verification of the End Effector**

**Design of gripper structure**

This study utilizes a gripper-style end-effector that combines gripping, harvesting, and transport functions. The design and optimization of the gripper structure are essential for effectively grasping and moving tobacco stems. After gripping and cutting the leaves, rapid transportation is needed, necessitating strong envelopment and structural rigidity. The fin-effect gripper must balance these functions through targeted design. An improved fin-effect gripper was developed, as illustrated in Fig. 3. The skeleton is made from thermoplastic polyurethane elastomer (TPU), which offers excellent elasticity and support, while the soft silicone contact surface securely envelops the tobacco leaves. The gripper features ribs that are thicker in the center and taper toward the edges, with outer joints designed to taper based on deformation needs and inner joints further thinned. This design aligns with the leaf stem's cross-sectional profile and the clamps' rigidity requirements.

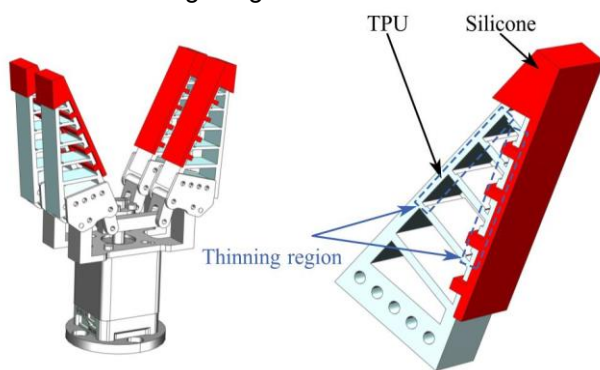


Fig. 3 – The structure design of fin gripper

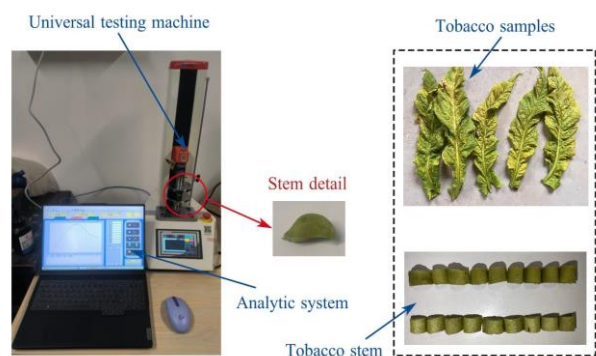


Fig. 4 – The physical properties testing of tobacco leaves and stems

**The material model parameters of tobacco**

The gripper structure is composed of two hyperelastic materials: TPU and silicone. The TPU material closely fits the second-order Mooney-Rivlin model, and its strain energy function is expressed as:

$$W = C_{10}(I_1 - 3) + C_{01}(I_2 - 3) \tag{1}$$

where  $W$  represents the strain energy, [MPa];  $C_{10}$  and  $C_{01}$  are material parameters, [MPa];  $I_1$  and  $I_2$  are the first and second strain invariants, respectively, with material parameters set as  $C_{10}=2.101\text{MPa}$  and  $C_{01}=0.105\text{MPa}$  (Guan Y. K. et al, 2023).

The second-order Yeoh model effectively characterizes silicone rubber, and its strain energy density function is expressed as:

$$W = C_{10}(I_1 - 3) + C_{20}(I_2 - 3)^2 \quad (2)$$

where  $C_{10}$  and  $C_{20}$  are material parameters set at 0.11 MPa and 0.02 MPa, respectively (Polygerinos P. et al, 2015).

The physical properties of tobacco leaf stems were determined through experimentation, with equipment and samples shown in Fig. 4. The tobacco leaves used in the experiment were collected from the Modern Tobacco Planting Demonstration Base in Malong District, Qujing City, Yunnan Province, China, and belong to the Yunyan 301 variety. Thirty mature and harvested tobacco leaves were randomly selected. The leaf blades were removed, retaining only the stems, which were cut into approximately 12 mm segments. Axial compression, radial compression, axial shear, and radial shear tests were conducted on the leaf stems using an electronic universal testing machine (ZQ-990). The density of the leaf stems was measured using the drainage method with an electronic balance (LQ-C20002) and a graduated cylinder. Due to slight variations in the shape and size of the test stems, each test was repeated 10 times, and the average value was calculated. The leaf stems were assumed to be transversely isotropic, meaning the radial and chord directions share the same modulus parameters. The final physical property parameters of the leaf stems are shown in Tab. 1, and Poisson's ratio was calculated using the following equations:

$$v_{xy} = \frac{E_x}{2G_{xy}} - 1 = v_{xz} \quad (3)$$

$$v_{yz} = \frac{E_y}{2G_{yz}} - 1 \quad (4)$$

Table 1

The physical property parameters of tobacco leaves and stems

| Parameters | Elastic modulus [MPa] |           | Shear modulus [MPa] |          | Poisson's ratio |          | Density [kg·m <sup>-3</sup> ] |
|------------|-----------------------|-----------|---------------------|----------|-----------------|----------|-------------------------------|
|            | $E_x$                 | $E_y/E_z$ | $G_{xy}/G_{xz}$     | $G_{yz}$ | $v_{xy}/v_{xz}$ | $v_{yz}$ | $\rho$                        |
| Values     | 5.34                  | 3.95      | 1.93                | 1.84     | 0.38            | 0.07     | 993.30                        |

### Finite element analysis of clamping force

Nonlinear static analysis was conducted using ANSYS Workbench. A simplified clamp model was imported, focusing on the clamping and wrapping behavior on the left side of the tobacco stem. Fillets and small step features were removed, and material connections were simplified to surface contact for enhanced computational efficiency. New materials were defined in the material library based on the given parameters and assigned to each part of the clamp. Friction contact was established between the silicone and the surface of the tobacco stem, while bonded contact was defined between the inner silicone surface and the TPU. A nonlinear meshing strategy was applied, generating first-order hexahedral elements to ensure computational efficiency and stability. To determine the optimal clamping force of the redesigned clamp, a fixed constraint was applied to the cylindrical hole of the clamp, while a lateral displacement constraint was added at the base of the stem. A clamping force was then applied on the opposite side of the stem, and the effects of clamping forces of 2 N, 2.5 N, and 3 N were explored. An integral solution method was used, accounting for large deformation, with nonlinear control implemented using the asymmetric Newton-Raphson method. The final solution met the force convergence criterion.

The displacement cloud diagrams of stable clamping under different forces are shown in Fig.5. It illustrates that as the clamping force increases, the enveloping capacity improves. Due to the large curvature of the outer contour of the leaf stem, achieving complete envelopment is challenging. Further modification of the clamp's size parameters to achieve full envelopment would result in excessive deformation and may cause the left and right jaws to collide. Therefore, this study improved the overall stiffness of the clamp while maximizing its envelopment of the leaf stem. Fig. 5 shows that under the studied clamping forces, the clamp envelops most of the outer edge of the leaf stem's left side, achieving overall good coverage. Additionally, because of the small transverse thickness of the leaf stem, excessive clamping force may cause the jaws to collide. At a clamping force of 2.5 N, the line connecting the top and bottom of the clamp passes through the long axis of the stem's cross-section, indicating the critical force at which the jaws might collide. Therefore, the clamping force should be kept at  $\leq 2.5$  N.

To further investigate the clamp's stiffness, the equivalent strain cloud diagrams under different clamping forces were obtained, as shown in Fig.6. It illustrates that the equivalent strain distribution in the contact area is relatively uniform, with higher equivalent stress at each joint, reaching a maximum of 0.24 m/m under a 3 N clamping force. Additionally, the greater the clamping force, the larger the equivalent strain in the contact area between the clamp and the leaf stem, resulting in greater elastic recovery energy and improved clamp stiffness. Based on the maximum force limit from the above analysis, a clamping force of 2.5 N provides sufficient stiffness to ensure stable tobacco leaf harvesting and retrieval. Therefore, this clamping force of 2.5 N was selected for subsequent harvesting tests.

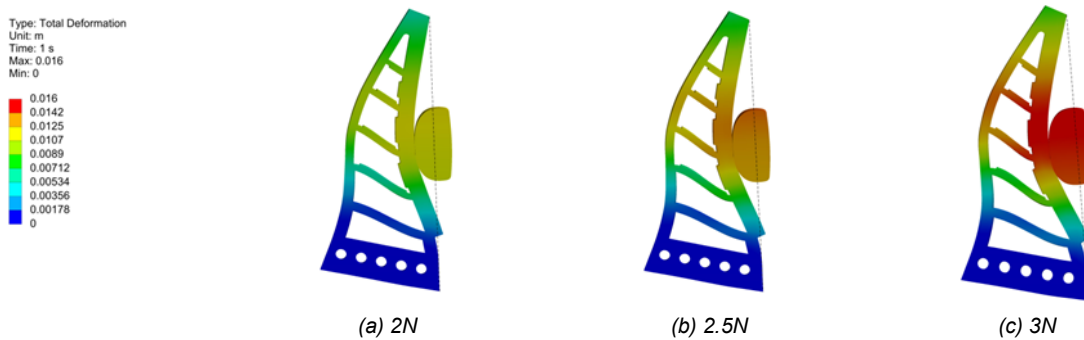


Fig. 5 – The displacement cloud diagrams of clamped leaf stems under different forces

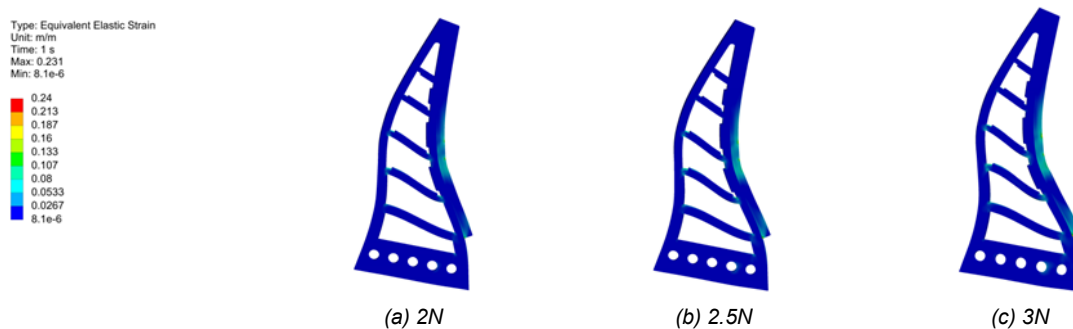


Fig. 6 – The equivalent strain cloud diagrams of clamped leaf stems under different clamping forces

**The motion analysis of robotic arm**

**The structure and parameter design**

The tobacco leaves harvesting robot uses the AUBO-I5 robotic arm, with its key parameters listed in Tab. 2. As shown in Tab. 2, the robotic arm has a working radius of 886.5 mm, while the average height of the tobacco leaves is approximately 1.5 m. Since tobacco plants mature gradually from top to bottom over 1-2 months, with only 2-3 leaves harvested at the same height during each picking cycle, a single robotic arm cannot meet agronomic needs. In this study, a 6+1 axis robotic arm solution was implemented, adding an 800 mm adjustable sliding platform at the base of the robotic arm. This setup allows the adjustment of the arm's workspace to meet the agronomic requirements for layered tobacco leaf harvesting, while keeping the slide's position fixed during the process.

**Table 2**

**The parameters of the AUBO-I5 Robotic Arm**

|                                      |                      |                             |                      |                      |                      |
|--------------------------------------|----------------------|-----------------------------|----------------------|----------------------|----------------------|
| Max load                             | 5 kg                 | Weight                      | < 24 kg              | Free load ratio      | < 4.8                |
| Degrees of Freedom                   | 6                    | Repeat positioning accuracy | ±0.02 mm             | Working radius       | 886.5 mm             |
| <b>Maximum velocity of each axis</b> |                      |                             |                      |                      |                      |
| <b>J<sub>1</sub></b>                 | <b>J<sub>2</sub></b> | <b>J<sub>3</sub></b>        | <b>J<sub>4</sub></b> | <b>J<sub>5</sub></b> | <b>J<sub>6</sub></b> |
| 223 °/s                              | 223 °/s              | 223 °/s                     | 237 °/s              | 237 °/s              | 237 °/s              |

**Workspace Analysis**

The AUBO-I5 robotic arm features six degrees of freedom, with the first three controlling the end-effector's position and the latter three its orientation. A fixed coordinate system was established for the links to describe each joint's motion in three-dimensional space, with the joint posture represented by its coordinate system position. The kinematic model was derived using homogeneous coordinate transformation, employing the modified Denavit-Hartenberg (M D-H) method for the forward kinematic model.

$$\begin{aligned}
 {}^{i-1}T_i &= \begin{bmatrix} c\theta_i & -s\theta_i & 0 & a_{i-1} \\ s\theta_i c\alpha_{i-1} & c\theta_i c\alpha_{i-1} & -s\alpha_{i-1} & -s\alpha_{i-1}d_i \\ s\theta_i s\alpha_{i-1} & c\theta_i s\alpha_{i-1} & c\alpha_{i-1} & c\alpha_{i-1}d_i \\ 0 & 0 & 0 & 1 \end{bmatrix} & {}^0T_1 &= \begin{bmatrix} 1 & 0 & 0 & 0 \\ 0 & 1 & 0 & 0 \\ 0 & 0 & 1 & d_1 \\ 0 & 0 & 0 & 1 \end{bmatrix} & {}^1T_2 &= \begin{bmatrix} c_2 & -s_2 & 0 & 0 \\ 0 & 0 & -1 & -0.122 \\ s_2 & c_2 & 0 & 0 \\ 0 & 0 & 0 & 1 \end{bmatrix} \\
 {}^2T_3 &= \begin{bmatrix} c_3 & -s_3 & 0 & 0 \\ 0 & 0 & 1 & 0.1215 \\ -s_3 & c_3 & 0 & 0 \\ 0 & 0 & 0 & 1 \end{bmatrix} & {}^3T_4 &= \begin{bmatrix} c_4 & -s_4 & 0 & 0.408 \\ -s_4 & c_4 & 0 & 0 \\ 0 & 0 & -1 & 0 \\ 0 & 0 & 0 & 1 \end{bmatrix} & {}^4T_5 &= \begin{bmatrix} c_5 & -s_5 & 0 & 0.376 \\ -s_5 & -c_5 & 0 & 0 \\ 0 & 0 & -1 & 0 \\ 0 & 0 & 0 & 1 \end{bmatrix} \\
 {}^5T_6 &= \begin{bmatrix} c_6 & -s_6 & 0 & 0 \\ 0 & 0 & 1 & 0.1025 \\ -s_6 & -c_6 & 0 & 0 \\ 0 & 0 & 0 & 1 \end{bmatrix} & {}^6T_7 &= \begin{bmatrix} c_7 & -s_7 & 0 & 0 \\ 0 & 0 & -1 & -0.094 \\ s_7 & c_7 & 0 & 0 \\ 0 & 0 & 0 & 1 \end{bmatrix}
 \end{aligned} \tag{5}$$

where,  $s_i$  and  $c_i$  represent  $\sin\theta_i$  and  $\cos\theta_i$ , respectively.

Multiplying the above matrices in sequence on the right yields the robot's forward kinematics expression.

$${}^0T_7 = {}^0T_1 {}^1T_2 {}^2T_3 {}^3T_4 {}^4T_5 {}^5T_6 {}^6T_7 \tag{6}$$

Fig.7(a) illustrates the model diagram and the coordinate systems for each joint, while Tab.3 lists the corresponding D-H parameters. The M D-H method provides the coordinate transformation matrix for the homogeneous transformation from coordinate system  $i$  to system  $i-1$  (Peng J. et al., 2019).

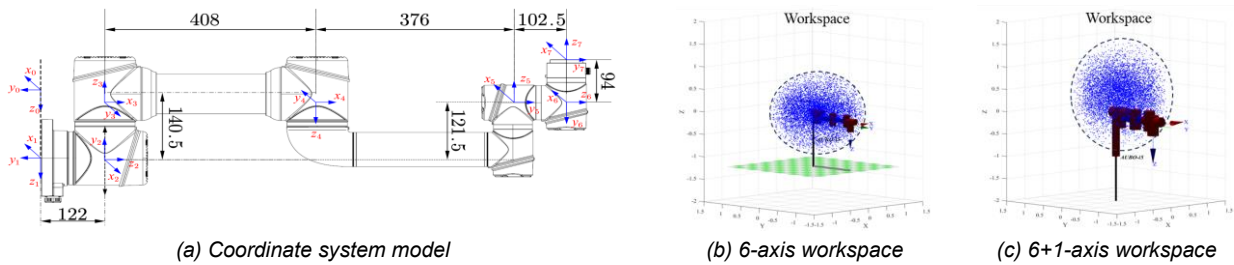


Fig. 7 – AUBO-I5 robot model and workspace

Table 3

The M D-H parameters of 6+1 axis robotic arm

| Link $i$ | $a_{i-1}$ [mm] | $\alpha_{i-1}$ [°] | $d_i$ [mm] | $\theta_i$ [°] | Variation range |
|----------|----------------|--------------------|------------|----------------|-----------------|
| 1        | 0              | 0                  | $d_1$      | 0              | 0-800 mm        |
| 2        | 0              | 90                 | 122        | $\theta_1$     | $\pm 360^\circ$ |
| 3        | 0              | -90                | 121.5      | $\theta_2$     | $\pm 175^\circ$ |
| 4        | 408            | 180                | 0          | $\theta_3$     | $\pm 175^\circ$ |
| 5        | 376            | 180                | 0          | $\theta_4$     | $\pm 175^\circ$ |
| 6        | 0              | -90                | 102.5      | $\theta_5$     | $\pm 175^\circ$ |
| 7        | 0              | 90                 | 94         | $\theta_6$     | $\pm 360^\circ$ |

In Matlab, the Link and SerialLink functions were used to create a simplified model of the robotic arm's links. The simplified teaching model is shown in Fig. 7(a). The Monte Carlo method was used to simulate and analyze the robot's workspace, generating random values for each joint variable (Li J. et al, 2023):

$$\theta_i = \theta_{i_{\min}} + (\theta_{i_{\max}} - \theta_{i_{\min}}) \times \text{rand}(N,1) \tag{7}$$

Substituting the joint variables into the forward kinematics equation produces a point cloud map of the robot's workspace, as shown in Fig. 7(b) and 7(c). From the workspace point cloud, it is evident that without the sliding device, the workspace of the AUBO-I5 robotic arm is circular. With the 6+1 axis structure and the sliding device, the workspace becomes elliptical. This expanded workspace covers a larger area, meeting the height requirements for tobacco leaf picking by covering most of the plant's height. Additionally, the workspace analysis provides a theoretical basis for path planning and collision warning of the gripper.

### Tobacco leaf recognition and positioning

The visual recognition system consists of an Intel RealSense D435i depth camera and an Nvidia Jetson Nano platform. The D435i camera, with a depth range of 0.1 to 10 m, captures tobacco leaf images, while the Jetson Nano, powered by a quad-core processor and CUDA GPU, handles deep learning tasks.

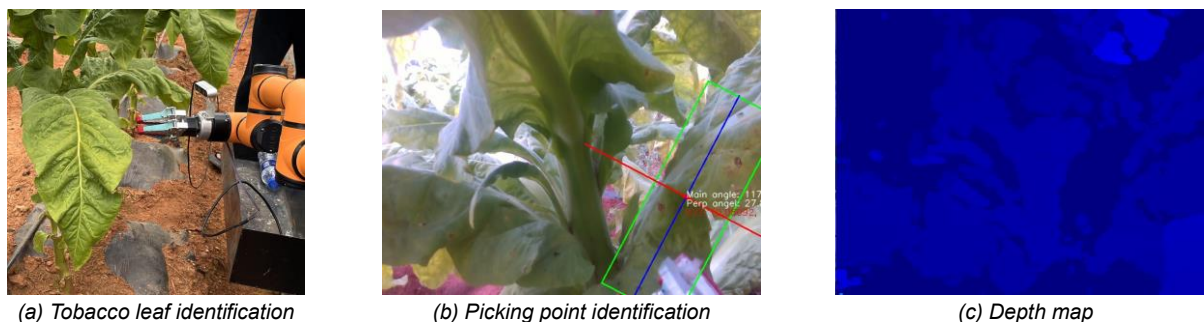


**Fig. 8 – Visual system recognition and positioning**

YOLOv7, a fast and accurate object detection algorithm, is used for real-time tobacco leaf recognition. The system captures images, processes them through YOLOv7's convolutional layers for feature extraction, and detects leaf stems using an Anchor-Free mechanism to generate bounding boxes. After non-maximum suppression, the system outputs the optimal coordinates for guiding the robot arm in precise picking. The method's high recognition accuracy and real-time performance make it suitable for complex field environments. To further enhance YOLOv7's accuracy, data augmentation, attention mechanisms, loss function refinements, and model integration were employed. The results of the visual recognition system are shown in Fig. 8.

## RESULTS

### Experimental conditions

The field test for tobacco leaf picking was conducted from August 14 to 16, 2024, in the modern tobacco leaf production demonstration area in Malong District, Qujing City, Yunnan Province. The test subjects were tobacco plants of the Yunyan 301 variety grown in the demonstration area. The test process is illustrated in Fig. 9.



**Fig. 9 – Tobacco leaf harvesting field experiment**

To evaluate the tobacco leaf picking performance of the entire machine, the time taken to fully pick a single leaf was used as a measure of overall picking efficiency. During preliminary testing, it was observed that jitter at the end of the robotic arm affected the recognition efficiency of the vision system. Therefore, the efficiency test was conducted at five speed levels: 20%, 40%, 60%, 80%, and 100% of the maximum movement speed of the robotic arm (the maximum linear speed and acceleration of the arm's end were 1.5 m/s and 1 m/s<sup>2</sup>, respectively). The picking time at each speed level was recorded. To eliminate the effects of lighting variations, all tests were scheduled for the morning of the same day. Each speed level was tested by picking 10 tobacco leaves, and the average picking time was calculated over 50 tests. The picking success rate was used to evaluate the machine's reliability. Tests were conducted in both the morning and afternoon. Five camera exposure times—10000  $\mu$ s, 25000  $\mu$ s, 40000  $\mu$ s, 55000  $\mu$ s, and 70000  $\mu$ s—were selected as factors for exploration. At each exposure level, 30 tobacco leaves were picked, and the success rate was calculated over 150 tests.

**Effect of robotic arm velocity on picking efficiency**

The results of the tobacco leaf picking test at different robotic arm speeds are summarized in Tab. 4. As the robotic arm speed increased from 0.3 m/s to 1.5 m/s, the average picking time dropped significantly from 9.00 seconds to 2.47 seconds, indicating a clear downward trend. Variance analysis of the robotic arm speed revealed significant differences between groups ( $P < 0.001$ ). Therefore, the speed of the robotic arm has a highly significant effect on the tobacco leaf picking time. As the robotic arm speed increases, the amplitude of vibrations at the arm’s end increases, potentially affecting the efficiency of the vision system's recognition. In practical picking, a balance must be struck between recognition efficiency and picking success rate. This is primarily because tobacco leaves near the plant may overlap or intertwine, and if the robotic arm moves too quickly, it could damage the surrounding leaves. Therefore, an efficient and relatively stable speed of 1.2 m/s was selected for subsequent experiments, ensuring maximum picking efficiency without compromising accuracy.

**Table 4**

**The test results of tobacco leaf picking efficiency at different robot arm speeds**

| No. | Mechanical arm speed [m/s] | Average picking time [s] | Variance |
|-----|----------------------------|--------------------------|----------|
| 1   | 0.3                        | 9.00                     | 0.37     |
| 2   | 0.6                        | 6.75                     | 0.13     |
| 3   | 0.9                        | 5.22                     | 0.03     |
| 4   | 1.2                        | 3.71                     | 0.01     |
| 5   | 1.5                        | 2.47                     | 0.04     |

**Effect of exposure time on picking success rate**

Exposure time is a crucial parameter for calibrating the visual recognition system. To investigate the effect of varying exposure times on picking success rates while accounting for changes in ambient light intensity during actual harvesting, experiments were conducted at 8 a.m. and 2 p.m., reflecting different ambient light conditions. The test data and pictures are shown in Tab. 5 and Fig. 10 respectively.

**Table 5**

**Experimental results on tobacco leaf picking success rate under different exposure times**

| Exposure time [μs] | Picking success rate (a.m) [%] | Picking success rate (p.m) [%] |
|--------------------|--------------------------------|--------------------------------|
| 10000              | 33.67                          | 43.33                          |
| 25000              | 63.33                          | 60.00                          |
| 40000              | 90.00                          | 83.33                          |
| 55000              | 73.33                          | 66.67                          |
| 70000              | 53.33                          | 46.67                          |



**Fig. 10 – Tobacco leaf harvesting picture under different exposure times**

The results indicate that there are significant differences in picking success rates across various exposure times, regardless of the time of day. The variance analysis results show  $P < 0.001$ , indicating an extremely significant effect. In the morning, when the exposure time was set to 40000 μs, the picking success rate peaked at 90.00%. In the afternoon, under the same exposure time, the picking success rate also reached a peak of 83.33%. Overall, variations in ambient light intensity significantly influenced the picking success rates at the same exposure time. Under poor ambient lighting conditions, the upper limit of the picking success rate may be restricted. Therefore, selecting appropriate harvesting times and weather conditions is crucial. In conclusion, selecting an appropriate exposure time can significantly enhance the system’s ability to identify tobacco leaves, ultimately improving the picking success rate. The tobacco leaf picking robot system developed in this study, based on machine vision, demonstrates excellent picking performance.

## CONCLUSIONS

This study developed an intelligent, non-destructive tobacco leaf picking robot utilizing machine vision. The research focused on the design and analysis of key components, with field experiments conducted to assess the machine's overall picking performance. This research yielded the following conclusions:

(1) The clamping jaw structure was redesigned based on the fin-ray effect. Finite element analysis revealed that increasing the clamping force improves the jaw's wrapping capability. To prevent collisions while maintaining sufficient rigidity and stability during tobacco leaf picking and collection, the clamping force was set to 2.5 N.

(2) The working space of the robot arm without the sliding table is circular, while the 6+1-axis arm with the sliding table has an elliptical workspace. This larger range covers most of the tobacco plant height, meeting the operational requirements for leaf picking.

(3) The speed of the robotic arm significantly impacts the picking time ( $P < 0.001$ ). At 1.5 m/s, the average picking time was minimized to 2.47 seconds. A speed of 1.2 m/s was found to balance efficiency and picking success rate.

(4) Exposure time significantly affects the picking success rate ( $P < 0.001$ ). A 40000  $\mu$ s exposure achieved a peak success rate of 90.00% in the morning and 83.33% in the afternoon. Overall, changes in ambient light intensity noticeably impacted success under the same exposure conditions.

## ACKNOWLEDGEMENTS

The study was funded by China National Tobacco Corporation Yunnan Provincial Company Project "Research and Application of Key Technologies for Automated Tobacco Leaf Picking and Editing Based on Image Recognition" (2023530000241021), Chongqing Education Commission Science and Technology Research and Technology Youth Fund Project (KJQN202400208) and Research Project of Beibei District, Chongqing (2024-05).

## REFERENCES

- [1] Bu, L. X., Chen, C. K., Hu, G. R., Sugirbay, A., Chen, J., (2020). Technological Development of Robotic Apple Harvesters: A Review (苹果收获机器人技术发展综述). *INMATEH-Agricultural Engineering*, 61(2): 151-164.
- [2] Guan Y. K., Hou Z. G., Hu B., Cong X. P., Lyu C. L., (2023). Design and Experimental Research of Flexible Gripper Based on Fin Ray Effect (基于鳍条效应的柔性夹爪设计与试验研究). *Machine Tool & Hydraulics*, 51(04): 86-91.
- [3] He, Z., Ding, X. T., Li, K., Shi, Y. G., Cui, Y. J., (2023). Design and Experiment of End Effect for Kiwifruit Harvesting Based on Optimal Picking Parameters (基于最优采摘参数的猕猴桃采摘末端执行器设计与试验). *INMATEH-Agricultural Engineering*, 69(1), 325-334.
- [4] Jin Y. J., (2020). Recognition Technology of Agricultural Picking Robot Based on Image Detection Technology (基于图像检测技术的农业采摘机器人识别技术). *INMATEH-Agricultural Engineering*, 62(3): 191-200.
- [5] Li Y., Chu J. K., Yu J., (2022). Effect of Ditching on Seedling Quality and Mechanical Transplanting of Drill Seedlings Under Low Sowing Quantity (烟草收获机采摘机构对烟叶采收效果影响的研究). *Journal of Agricultural Mechanization Research*, 44(12): 170-174+181.
- [6] Liu, S., Wang, J., Mou, H., Fan, L., Fu, S., Zhu, C., (2020). Design and Experiment of Moving along Ridge Control System for Tobacco Picking Machine (烟叶采收机仿垄行走控制系统设计与试验). *Transactions of the Chinese Society of Agricultural Engineering*, 31(S2):83-87.
- [7] Li, J., Zhao, Q., Li, L. J., Wu, Z. C., Guo, X., (2023). Trajectory Planning of Camellia Oleifera Pollen Picking Manipulators Based on an Improved Particle Swarm Optimization Algorithm (基于改进粒子群算法的油茶花粉采摘机械臂轨迹规划). *Journal of Mechanical Transmission*, 47(2): 86-92.
- [8] Ma, S. J., Zhu, C. H., Zhang, C. C., Ran, Y. L., Li, B. Q., Wang, W. Z., (2024). Design and Experimental Research on Picking Mechanism of Self-propelled Tobacco Leaf Picking Machine (自走式烟叶采摘机采摘机构的设计与试验). *Journal of Agricultural Mechanization Research*, 46(03): 120-127.
- [9] Peng, J., Ding, Y., Zhang, G., Ding, H., (2019). An Enhanced Kinematic Model for Calibration of Robotic Machining Systems with Parallelogram Mechanisms. *Robotics and Computer-Integrated Manufacturing*, 59: 92-103.

- [10] Polygerinos, P., Wang, Z., Overvelde, J. T., Galloway, K. C., Wood, R. J., Bertoldi, K., Walsh, C. J. (2015). Modeling of Soft Fiber-Reinforced Bending Actuators. *IEEE Transactions on Robotics*, 31(3): 778-789.
- [11] Shu, Y., Zheng, W., Xiong, C., Xie, Z., (2024). Research on the Vision System of Lychee Picking Robot Based on Stereo Vision. *Journal of Radiation Research and Applied Sciences*, 17(1): 100777.
- [12] Yu Y. C., Wei F. D., Qin W. Y., Liu T., Zeng M., Ning W. Y., (2016). Technology Development of Tobacco Harvester (烟草收获机技术发展概述). *Journal of Agricultural Mechanization Research*, 38(02): 255-262.